Silicon
https://doi.org/10.1007/s12633-023-02396-5

ORIGINAL PAPER

New Insights Into Method Development and Characterization of Amorphous Silica From Wheat Straw

Sangeetha Piriya Ramasamy[1,2] · Davamani Veeraswamy[2] · Parameswari Ettiyagounder[2] · Lakshmanan Arunachalam[3] · Sivakumar Senjeriputhur Devaraj[4] · Kadirvelu Krishna[5] · Sadish Oumabady[6,7] · Ruben Sakrabani[1]

Received: 22 January 2023 / Accepted: 7 March 2023

Abstract
Amorphous silica, a specialised silicate adsorbent is extensively extracted from agricultural residues for application in various environmental domains. Wheat straws are a rich source of silica that have earlier been overlooked however demand for value addition. The study presents an innovative approach to extracting silica from wheat straw and standardising the extraction process to produce clean product. The sodium silicate solution and the amorphous silica synthesis were obtained by modifying the template mediated sol–gel method. Optimum temperature, concentration and pH were identified for the cleaner production of silica with maximum yield and favourable adsorbent characteristics. The crystallographic properties analysed by the X-Ray Diffraction revealed the amorphous nature of silica extracted from ash at 650 °C for 4 h. The structure of phytolith present in the wheat straw was observed in the form of articulated elongate undulate epidermal phytolith under scanning electron microscopy. The Energy Dispersive X-ray spectrum exhibited higher amount of silica (Si %) of 70.10% with a minimal percentage of potassium (9.96%). The sharp bend at 1025 cm^{-1} is attributed to the siloxane (Si–O-Si) vibrations in Fourier transform infrared spectroscopic graph of amorphous silica. The specific surface area measurements of amorphous silica showed type II isotherm curve with a hysteresis of H3 type. The optimum conditions derived to produce amorphous silica were 3 M NaOH and 3 M H_2SO_4 at pH 9.

Keywords Wheat straw · Amorphous silica · Phytolith · Sol gel template method · Method standardization

1 Introduction

Improper waste management is a significant challenge facing the agricultural sector worldwide. Agricultural waste ranks second in quantity among the waste generated in food supply chains. Post-harvest activities, as well as the sorting and grading of fruits and vegetables, contribute to an estimated food wastage of 7.5–17.5% [1, 2]. An effective solution to this issue involves in the conversion of agricultural waste into bio-based products and energy resources. A large amount of agricultural waste are produced globally with major contributions from rice straw (731 MT), wheat straw (354 MT), corn straw (203 MT) and sugarcane bagasse (180 MT) [3]. Among these waste products, Europe is the largest producer of wheat straw, generating 132.59 Million Tonnes per year, which accounts for 37% of the total waste. Furthermore, Europe, Asia, and America are the primary producers of wheat straw, accounting for 96% of global production [3, 4].

✉ Ruben Sakrabani
r.sakrabani@cranfield.ac.uk

1 School of Water, Energy and Environment, Cranfield University, Cranfield MK43 0AL, UK

2 Department of Environmental Sciences, Tamil Nadu Agricultural University, Tamil Nadu, Coimbatore 641 003, India

3 Department of Nano Science and Technology, Tamil Nadu Agricultural University, Tamil Nadu, Coimbatore 641 003, India

4 Department of Agronomy, Tamil Nadu Agricultural University, Tamil Nadu, Coimbatore 641 003, India

5 Defence Research and Development Organisation, Bharathiar University, Tamil Nadu, Coimbatore 641 046, India

6 School of Biological Sciences, Institute for Global Food Security, Queen's University, Belfast BT9 5DL, Northern Ireland, UK

7 Department of Environmental Science, Dr. Y S Parmar University of Horticulture and Forestry, Himachal Pradesh 173 230 Nauni, India

Published online: 22 March 2023

Improper disposal of agricultural residue through burning and indiscriminate dumping poses a significant threat to both human health and the environment. Furthermore, it undermines food and energy security. Developing countries are particularly affected by residue burning, which requires technological reforms and regulatory support [5]. Additionally, the underutilization of waste straw has negative environmental effects, as it accelerates the emission of carbon dioxide when left to decompose in the soil. The substantial burning of biomass in 2014–2015 in India resulted in alarming levels of air pollution and prompted various organizations to address the issue of waste disposal [6]. Consequently, there is a growing need to manage and handle waste as a resource with zero burden. Identifying ways to minimise the degradation of natural ecosystems while preserving resources presents an opportunity to move towards a sustainable and circular economy [7]. Researchers are currently exploring novel strategies for waste valorisation in food supply chains, focusing on developing policies that create circular loops in waste management and converting waste into valuable products. Value-added waste can be used to create commercial products, offering a potential opportunity for researchers, industries and farmers.

Biomass and agricultural residue are new age renewable sources that can be used as energy precursors through various thermochemical conversion methods such as pyrolysis, hydrothermal carbonization, torrefaction, and gasification [8]. The widespread availability of biomass makes it suitable for a range of industrial applications in terms of energy, effluent treatment and controlling GHG emissions. In particular, straws have potential for comprehensive utilization and generating various opportunities for valorization. In addition to their organic composition, the presence of inorganic constituents can also be exploited to produce materials with higher efficacy and value. Silicon dioxide (SiO_2) is an important inorganic constituent in biomass, with silica (Si) in plants in the form of silicic acid (H_4SiO_4) during the growth period. This Si polymerises and precipitates as amorphous silica (ASi) in the plants. As plants decay in the natural environment, the biogeochemical cycle of Si allows for the investigation and use of phytolith silica [9]. The highly ordered SiO_2 framework provides a simple structure for the preparation of templating agents [10], cementitious material [11] and energy purpose [12]. Recent research has highlighted the demand for biomass-derived materials and their critical findings in this context. A suitable preparatory process can transform Si into a product with multifunctional applications. Eco-production of Si from biomass fosters circular economy that reduces environmental impacts and increases efficiency through resource utilization. With this background, the current study hypothesises that characterisation of ASi from wheat straws, specifically standardising the modified sol–gel method and its chemical characteristics for various environmental applications are comparable to commercial amorphous silica (CSi). As there are few reports on the utilization of wheat straws (Table 1) and their high silica content [13], this research would be novel in producing silica materials from them.

2 Experimental

2.1 Materials

Wheat straws used in the study were collected from the Rothamsted Research Centre, United Kingdom. Sodium hydroxide (> 99%), hydrochloric acid (35–37%), sulphuric acid (95–97%), n-butyl alcohol (> 99%), Cetyltrimethylammonium bromide (CTAB, > 98%) and commercial amorphous silica were purchased from Merck, United Kingdom. The solutions were prepared using deionised water (Milli-Q).

2.2 Silica Synthesis

2.2.1 Preparation of Wheat Straw Ash

Wheat straw was washed and dried at 60 °C for 48 h to remove the excess moisture. Upon drying, the straws were ground to small pieces (0.2 mm) and stored in airtight containers. The dried straw was burnt in a muffle furnace at 450, 650, 750, 850 and 950 °C for 4 h to produce ash. The ground powder was burnt at programmed muffle furnace with 10 °C min^{-1} rate of increase in three stages. In the first stage, the temperature was ramped to 250 °C and held for an hour, followed by a rise to 450 °C with a holding time of 1 h and finally to 650–950 °C and held for 4 h to remove carbon and organics. The obtained ash was sealed in zip lock bag and stored for estimating silica (Si) content, ash yield and other physico-chemical analysis.

Table 1 Percentage of SiO_2 in different biomass

Biomass	~SiO_2, %	Studies on the biomass mentioned
Corn leaf sheath	64.32	[14, 15]
Sugarcane baggase	73.00	[16]
Oil palm ash	46.00	[17]
Rice husk and Straw	93.00, 82.00	[18–20]
Bamboo leaf	57.40	[21]
Sorghum bicolor	88.75	[22]
Wheat straw	90.56	This study

2.2.2 Pre-treatment of Ash

The produced ash (200 g) was washed with 0.1 mol L^{-1} HCl (1000 mL) and kept shaking for 2 h. The suspension was then filtered and washed using deionised water. The solid residue was dried in hot air oven overnight at 120 °C and stored air tight for further process [23].

2.2.3 Sodium Silicate Production

The silicate solution was produced by modifying method of Okoronkwo et al. (2013b) (Fig. 1) [15]. The ash (50 g) was mixed with 3 M NaOH (500 mL) and continuously stirred at hot plate (4 h) to produce sodium silicate solution. To this, 100 mL of boiled distilled water was added. The solid portion was filtered out and the silicate solution (Na_2SiO_3) was saved for the production of amorphous silica [24].

2.2.4 Surfactant Mediated Amorphous Silica Production

Amorphous silica was produced by modifying Rovani et al. method (Fig. 1). In a beaker, 4.5 g of CTAB was added to a mixture of 1:1 H_2O and Butanol. The mixture was heated at 60 °C to which 40 mL of sodium silicate solution was added to form an emulsion under constant stirring. Later, 3 M of H_2SO_4 was added in drops to neutralize the alkalinity of the emulsion until the pH reached 4. The process resulted in the formation of gel that is aged for 8 h. The aged silica particles were washed with distilled water and filtered to obtain the silica particles. The ASi particles were then oven

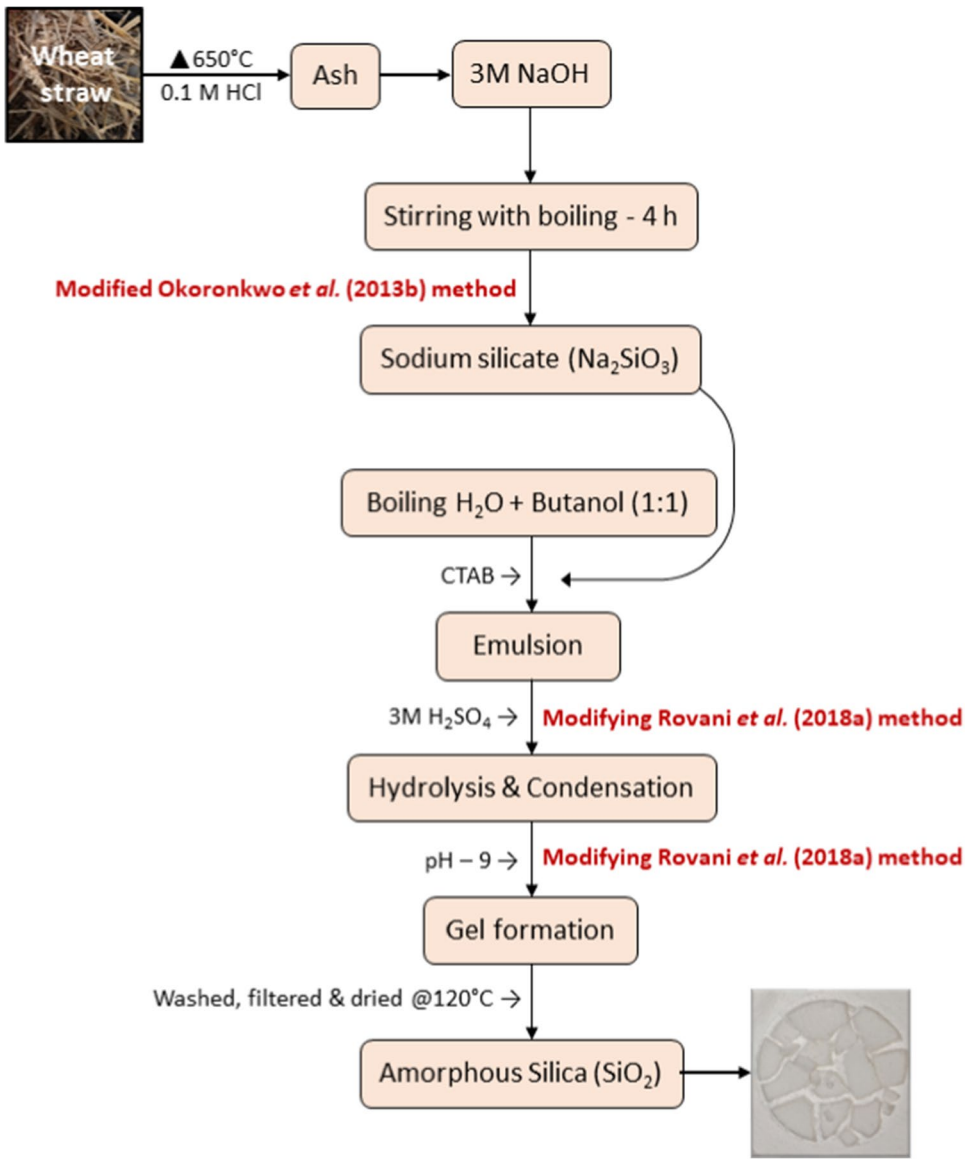

Fig. 1 Synthesis of amorphous silica using surfactant mediated method by Rovani et al. (2018a) [23] Okoronkwo et al. (2013b) [15]

dried at 120 °C [23]. The following equations represent the mechanism of silica particle formation [25].

$$SiO_2\ (s) + 2NaOH\ (aq.) \rightarrow Na_2SiO_3\ (aq.) + H_2O\ (l) \quad (1)$$

$$Na_2SiO_3\ (aq.) + H_2SO_4\ (aq.) \rightarrow SiO_2(s) + Na_2SO_4\ (aq.) + H_2O\ (l) \quad (2)$$

Amorphous silica yield: The amount of amorphous silica is determined by:

$$Yield\ (\%) = \frac{W_{ASi} \times 100}{W_A} \quad (3)$$

where, W_{ASi} is weight of amorphous silica and W_A is weight of ash.

2.2.5 Characterization

Proximate and ultimate analysis were performed for the straw and ash using standard procedures [26]. CHNS analysis was done using Elementor Vario III. The dissolved silica analysis in the samples were performed on a Perkin Elmer Optima 8300 ICP-OES at the wavelength 212.4 nm.

XRF (X-Ray Fluorescence) analysis was performed using Olympus DELTA Premium 600 Series. SEM (Scanning Electron Microscope) images were recorded on a tabletop microscope from TESCAN S8215G, focused ion beam field emission scanning electron microscope (FIB-FESEM), at a typical acceleration voltage of 12.0 kV. FTIR (Fourier Transform InfraRed Spectroscopy) graphs were performed using Shimadzu Attenuated Total Reflection (ATR) spectrometer and the surface functionalities were obtained over wavenumber range of 400 – 4000 cm^{-1} [27].

The specific surface area and pore distribution of samples were analyzed by Nitrogen adsorption – desorption isotherms at – 196 °C using a 3P Meso 222 Sorption Analyser (3P instruments). For the test, 0.5–1 g of ASi was degassed at 200 °C for 2 h under vacuum. The BET surface area was carried at a pressure range of 5 – 104.5 kPa. The pore volume was measured at $P/P_0 = 0.99$ using BJH plot [28]. TGA analysis were recorded in a thermogravimetric analyzer TGA/DTG from TGA 8000, PerkinElmer. In addition, commercial silica (CSi) was characterised to compare its characteristics with biomass derived amorphous silica.

3 Results and Discussion

3.1 Mechanisms and Novelty

In order to produce amorphous silica (ASi), a modified surfactant mediated sol gel technique was utilized. However, the exact amounts of NaOH and H_2SO_4 needed for the synthesis of ASi proved challenging to determine. To address this, a slight modification was made to the procedure used by Rovani et al. (2018) and Okoronkwo et al. (2013b), which is illustrated in Fig. 1, resulting in successful production of ASi.

To extract amorphous silica from wheat straw ash samples, they were first subjected to acid leaching to remove impurities such as salts, organic components, and other oxides. Alkali NaOH at a concentration of 1 M was then used to extract amorphous silica from the ash at high temperatures. The NaOH melted and dissolved the silica from the ash, forming sodium silicate (Na_2SiO_3), which was used as the source to produce amorphous silica. However, 1 M NaOH concentration was insufficient to react with Si in ash, so a higher concentration (3 M) was used until the reaction occurred. Similarly, 3 M of H_2SO_4 was able to produce silica precipitate instead of the initial concentration of 0.5 M (Fig. 1).

Amorphous silica (ASi) particles were produced using a surfactant-mediated sol–gel technique. Cetyltrimethylammonium bromide (CTAB) was utilized as the surfactant to serve as a template, while butanol was used as a co-surfactant to form a porous framework of ASi. CTAB prevented the agglomeration of Si particles, controlled their size, and created micelles in the solution [23]. The production mechanism of ASi involved hydrolysis, which led to the formation of silanol groups, followed by the condensation process where siloxane groups were formed using sulphuric acid in the presence of CTAB in a biphasic medium [29]. Therefore, using H_2SO_4 in co-condensation produced a white solid, which was filtered as amorphous silica (ASi).

4 Characterization of Biomass, Ash and Amorphous Silica

4.1 Thermal Properties

4.1.1 Proximate and Ultimate Analysis

The biomass underwent proximate analysis via combustion, which provided information on its volatiles (ASTM D3175-07), moisture (ASTM D3173-03), ash (ASTM D13174-07), and fixed carbon content (ASTM 3175–89), as summarized in Table 2. Similarly, the ultimate analysis was conducted to determine the carbon (C), hydrogen (H), nitrogen (N), and sulfur (S) content and compared to other biomass samples (Table 2). Notably, the results revealed that the produced wheat straw ash contained minimal carbon (0.15–0.25%) compared to the feedstock (38.86%).

The ultimate analysis further showed that the carbon (38.86%) was eliminated as CO_2 during combustion, decreasing to 0.07% (at 950 °C) in the ash. Additionally,

Table 2 Proximate analysis, elemental composition and dissolved silica content

This study					
Proximate analysis					
Sample	Moisture, %	Volatiles, %	Ash, %	Fixed carbon, %	
Wheat straw	13.11	79.78	5.48	14.72	
Dissolved Silica (mg L^{-1}) at different temperatures					
Wheat straw ash	650 °C	750 °C	850 °C	950 °C	
	15,008	1918	1069	567	
Ultimate analysis					
Sample	N%	C%	H%	S%	O%
Wheat straw	1.50	38.86	6.59	0.21	52.84
Ash @450 °C	0.25	1.42	0.99	0.16	97.18
Ash @650 °C	0.23	0.46	0.50	0.40	98.41
Ash @750 °C	0.19	0.18	0.23	0.39	99.01
Ash @850 °C	0.14	0.11	0.13	0.34	99.28
Ash @950 °C	0.15	0.07	0.12	0.31	99.35
Other research					
Rice straw [30]	0.2	37.19	4.8	0.3	57.6
Cogon grass [31]	0.9 ± 0.07	41.5 ± 0.06	5.3 ± 0.14	0.36 ± 0.005	51.9 ± 0.25
Corn cob [32]	2.4	46	6	0.5	37

the amount of hydrogen (6.59 to 0.12%) and nitrogen (1.50 to 0.14%) present in the biomass was reduced in the ash. In contrast, the oxygen percentage in the ash increased from 52.84% in wheat straw to approximately 99%. The CHNS results were consistent with those obtained from other residues such as rice, cogon grass, and corn cob utilized for silica synthesis (Table 2).

4.1.2 Ash Content and Chemical Composition

The elemental composition of wheat biomass and the ash obtained at various temperatures using XRF is presented in Table 3, indicating the presence of SiO_2, S, Fe, K_2O, CaO, MgO, Al_2O_3, and other elements in the ashes. It was evident that the percentage of SiO_2 increased significantly from wheat straw to ash and further to the ASi, which was attributed to the removal of volatile compounds during combustion. The highest SiO_2 content (30.20 ± 0.09%) was obtained at 650 °C, which was deemed suitable for the production of ASi.

Interestingly, the analysis revealed a unique interference of Al_2O_3 in the ASi samples, which was likely due to the use of aluminium foil during the calcination process. The silica crucibles can be used in place of aluminium foil. The acid washing of ash samples effectively removed other impurities, leading to negligible impurities in the amorphous silica. The presence of CaO, MgO, and K_2O in the ash was attributed to the use of fertilizers during wheat production and their uptake from the soil. Similar impurities were observed in silica produced from rice husk and straw [33]. However, the impurities in the ASi were much lower than those in palm kernel shells [34]. The acid

Table 3 Percentage composition of wheat straw, ash and amorphous silica

Sample	SiO_2 %	Fe %	K_2O %	CaO %	MgO %	Al_2O_3 %
Wheat straw	10.80 ± 0.06	0.37 ± 0.0038	2.01 ± 0.01	0.28 ± 0.012	0.18 ± 3.21	< LOD
Ash @450 °C	29.09 ± 0.09	0.95 ± 0.007	4.45 ± 0.01	0.96 ± 0.03	0.21 ± 1.14	< LOD
Ash @650 °C	30.20 ± 0.09	0.46 ± 0.007	7.53 ± 0.02	0.83 ± 0.03	0.23 ± 1.08	< LOD
Ash @750 °C	24.67 ± 0.08	0.49 ± 0.004	5.81 ± 0.02	0.68 ± 0.02	0.29 ± 1.09	< LOD
Ash @850 °C	25.11 ± 0.08	0.52 ± 0.001	5.43 ± 0.01	0.67 ± 0.02	0.22 ± 1.11	< LOD
Ash @950 °C	25.59 ± 0.08	0.45 ± 0.001	5.55 ± 0.01	0.65 ± 0.02	1.99 ± 1.14	< LOD
Amorphous silica (ASi)	34.41 ± 1.12	0.01 ± 0.002	< LOD	< LOD	0.19 ± 1.18	1.02 ± 0.44
Commercial silica (CSi)	79.09 ± 1.13	0.02 ± 0.002	< LOD	< LOD	0.22 ± 1.15	< LOD

*LOD-level of detection

pre-treatment of ash effectively removed impurities, resulting in the production of white ASi. The composition of CSi showed a higher SiO_2 content, likely due to the different source of Si and preparation method. However, other constituents in CSi were below the level of detection, similar to the ASi. These findings highlight the efficacy of acid washing in removing impurities from wheat straw ash to obtain high-quality ASi.

The Si content in wheat straw and ash was quantified using ICP-OES, with the results presented in Table 4. The SiO_2 concentration in the wheat straw was found to be lower than that in the ash produced at various temperatures. The amount of SiO_2 increased in the ash produced at 450 °C, followed by a decreasing trend after 650 °C. The temperature of 650 °C was determined to be the critical temperature for silica extraction from wheat straw for two primary reasons. First, based on elemental analysis, the residual carbon percentage was higher at 450 °C than at 650 °C. Second, temperatures higher than 650 °C resulted in crystalline silica, as confirmed by XRD analysis. The ICP-OES results showed that the SiO_2 content was minimal at 950 °C, which was also found to be unsuitable for extracting amorphous silica from rice husk ash [33].

The dissolved silica (mg L^{-1}) in the ash samples produced at different temperatures may vary significantly due to several factors. The solubility of silica is highly dependent on temperature, pH, and the presence of other chemical species. At higher temperatures, the solubility of silica generally increases, leading to a higher concentration of dissolved silica in the ash sample [35]. Additionally, the production temperature may affect the physical and chemical properties of the ash, which in turn can affect the solubility of silica. For example, at higher temperatures, the ash may have a higher degree of crystallinity or more stable mineral phases, leading to a lower concentration of dissolved silica. Similarly, the results of the dissolved silica test showed that the ash at 650 °C had higher (15,008 mg L^{-1}) dissolved silica than that at 950 °C (567 mg L^{-1}) (Table 2). On the other hand, at lower temperatures, the ash may be less crystalline and contain more amorphous silica, which is generally more soluble in water. Therefore, the big difference between the dissolved silica concentrations at different temperatures may be due to a combination of factors including solubility, mineralogy, and the physical and chemical properties of the ash produced at different temperatures. In contrast, the silica from oil palm kernel shells was extracted from the ash at 900 °C [34].

The higher amount of silica at 650 °C could be attributed to the temperature effect and the refractory nature of silica. At higher temperatures, the chemical reactions occurring during combustion are more intense and complete, leading to a greater release of SiO_2 from the biomass. However, as the temperature continues to rise, the SiO_2 in the biomass may start to volatilize and be emitted as gaseous silicon monoxide (SiO), which is more vulnerable to oxidation when entering the flue gas [36]. However, other factors, such as the composition and properties of the biomass, the specific combustion method, and the conditions of the combustion process, can also affect the amount of SiO_2 in the ash.

4.2 Visual Representations

Figure 2 displays digital images of the wheat straw and ash produced at various temperatures. The calcination process lasted for four hours and is reflected in the colour change of the samples. The ash obtained at 450 °C had a characteristic coarse, black texture, indicating incomplete combustion, which was confirmed by CHNS analysis. In contrast, the ash particles produced at 750 °C, 850 °C, and 950 °C had a slightly pinkish hue, similar to that of rice husks [33]. At 650 °C, white ash were observed with no incomplete combustion particles.

4.3 X-Ray Diffraction

The crystallographic characteristics of wheat straw and its resulting ash at varying temperatures were evaluated using X-ray diffraction (XRD) patterns, which are displayed in Fig. 3. The XRD patterns revealed the presence of quartz and tridymite (SiO_2) in the wheat straw at 21.2° and 26.6°, respectively. Upon subjecting the straw to high temperatures, the ash showed a reduction in the peak representing SiO2, with no tridymite peaks observed. The crystalline nature of the ash was found to decrease after combustion, but increased with increasing temperature. At higher temperatures, both amorphous and crystalline particles are generated during the combustion of organic material. As quartz is a crystalline form of Si, the ash possessed a higher crystallinity. Previous studies have indicated that extraction of silica

Table 4 ICP-OES results of Extractable Silica (SiO_2)

Sample		Wheat straw	Ash @450 °C	Ash @650 °C	Ash @750 °C	Ash @850 °C	Ash @950 °C
SiO_2 (mg Kg^{-1})	R_1	1338	3024	2236	1883	1779	1104
	R_2	1436	3047	2271	1788	2004	988
	R_3	1639	3229	2522	1531	1700	873
Average SiO_2		1471	3100	2343	1734	1827.67	988.34

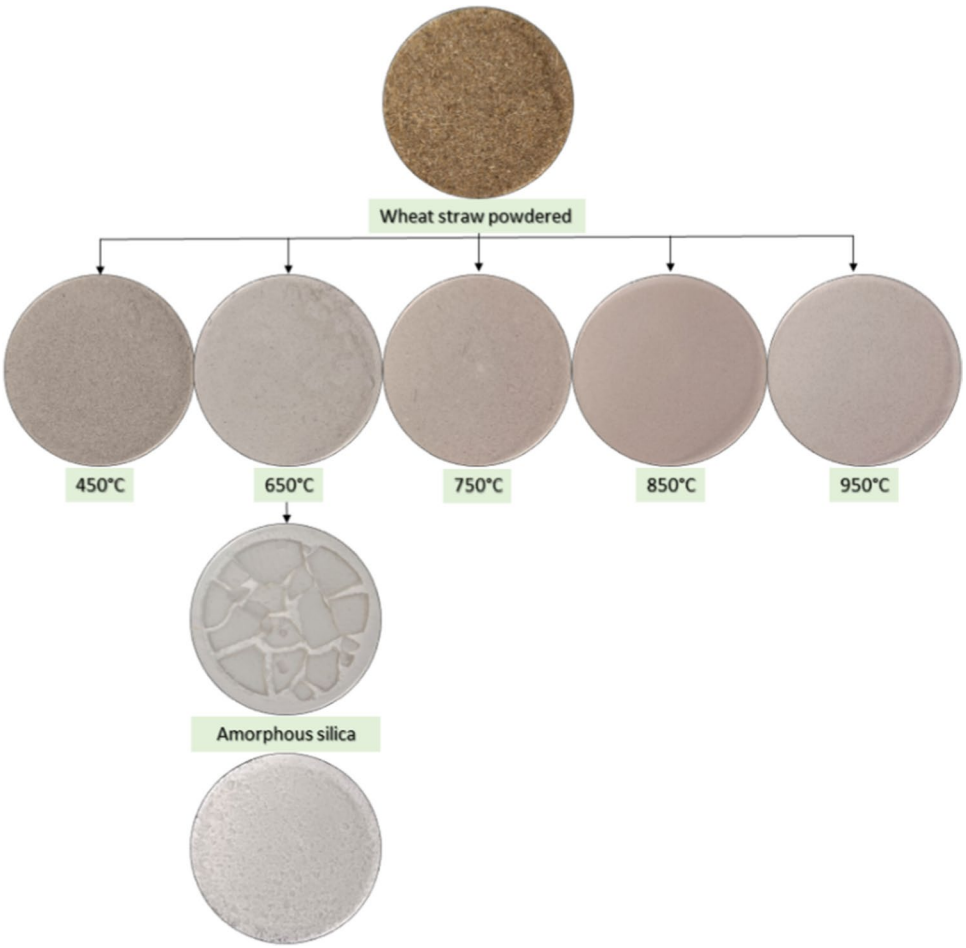

Fig. 2 Ash produced at different temperatures

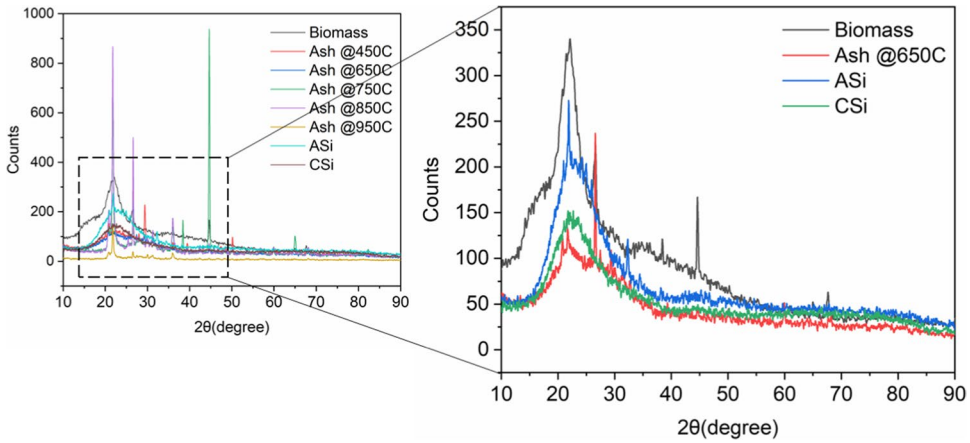

Fig. 3 XRD spectrum of wheat biomass, ash, ASi and CSi

at temperatures above 700 °C may not produce amorphous silica in its optimal form [37–39].

Furthermore, the XRD patterns revealed that the narrow and sharp peaks of ASi were converted to broad peaks, indicating an amorphous nature. The ASi pattern was similar to the CSi pattern throughout the entire range, indicating a high abundance of SiO_2 in the wheat straw, ash, and ASi. The presence of Si in all samples was confirmed through XRF analysis. Additionally, FTIR confirmed the presence of silanol groups on the surface of the particles. These results differed from the patterns observed in palm kernel shells and thermally generated palm kernel ash [34, 40]. The XRD analysis of amorphous silica (ASi) from agricultural residue can provide valuable information about the changes in its structure, stability, and durability under different conditions of temperature and pressure. The XRD pattern can also

indicate the purity of the material and its suitability for specific applications [41]. This information can help optimize the performance of ASi in various applications. For example, XRD analysis can reveal carbon sequestration measurements by minerals based on their crystalline structure.

4.4 Fourier Transform Infrared Spectroscopy

The FTIR spectrum of wheat straw, ash, and ASi were analyzed and presented in Fig. 4. The spectrum of ash obtained at different temperatures displayed various peaks of vibrations corresponding to functional groups. The ASi was found to be similar to the highly pure CSi (> 99%) throughout the pattern. The presence of CTAB molecules on the surface of SiO_2 were also observed. The bands at 2850 and 2900 cm^{-1} revealed the existence of CTAB on the surface of ASi with symmetric and asymmetric stretching of CH_2. However, no peaks at these bands were observed in the spectra of wheat straw and ash at different temperatures. Similar peaks were observed in the case of silica obtained from sugarcane bagasse [23].

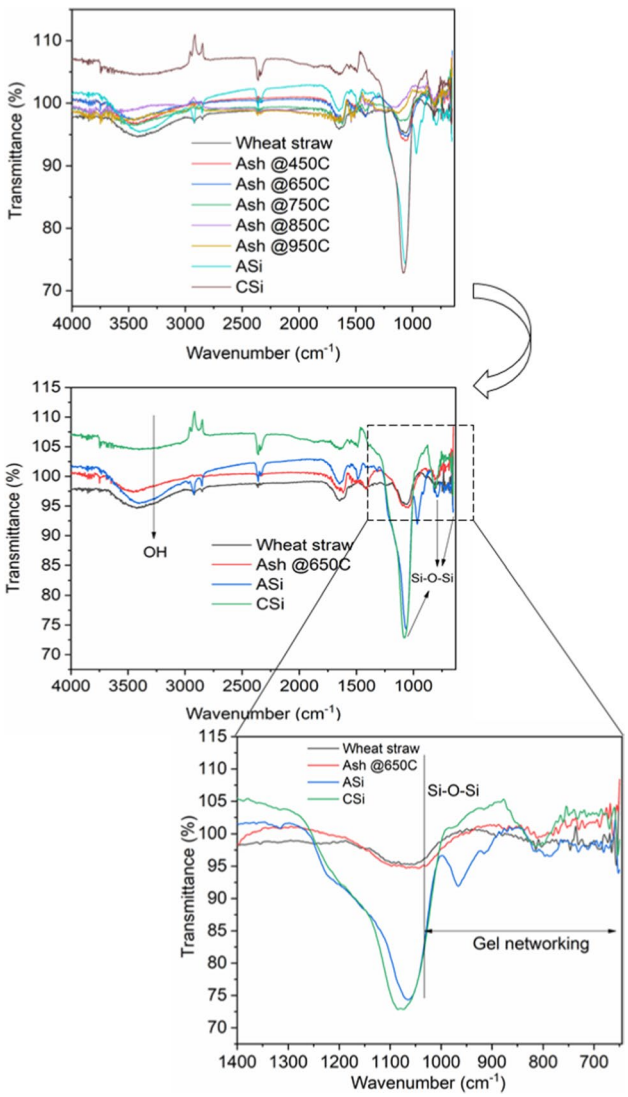

Fig. 4 FTIR spectrum of wheat biomass, ash, ASi and CSi

The broad band across 3200–3500 cm^{-1} depicted the O–H stretch of alcohol groups in all the spectra due to the adsorption or dehydration of water molecules on the surface [24]. The possible groups present were silanol (Si–OH) groups on the surface. The peak at 2850 cm^{-1} in wheat straw indicated the vibrations of C-H groups of cellulose and hemicellulose [33].

The spectra of ash obtained at different temperatures were different from the wheat straw. A wide difference in the band width was observed between the wheat straw (similar to ash) and ASi (similar to CSi) from 1000 to 1250 cm^{-1}. The sharp bend at 1025 cm^{-1} is attributed to the siloxane (Si–O-Si) vibrations. The band from 400 to 1000 cm^{-1} displayed the gel networking [42]. The evidence of predominant and strong asymmetric stretching of Si–O-Si at 795 cm^{-1} and a sharp peak at 466 cm^{-1} was assigned to Si–O symmetric stretching. These bands also represent the quartz mixture that was confirmed by the XRD pattern. The results were in agreement with palm kernel shell [34] and rice husk silica [43, 44].

The presence of silanol groups between 400 and 800 cm^{-1} are polar and hydrophilic, that can interact with other polar and hydrophilic substances, such as water molecules. As a result, silanol groups can be used for various applications, such as in catalysis, adsorption, and chromatography. The surface silanol (Si–OH) groups on surface of silica can be modified with various organic molecules through post-synthesis steps like silylation [45]. To understand and control the surface modification process, it is crucial to characterize the silanol chemistry. The silanol number, which is the number of Si–OH groups per unit surface area, has been studied extensively and is found to vary based on the type and history of the silica material [46]. Hydroxylation, which is the process of reacting siloxane (Si–O-Si) groups with water molecules, can increase the number of Si–OH groups and make the silica surface more hydrophilic [47]. This may impact how the material interacts with drug molecules during loading into the mesopores for controlled release applications or adsorption of polar molecules.

The unique peak at 700–800 cm^{-1} was noted for ASi and CSi, which corroborated the vibration of the Si–C group. The peak was also noticed for Si derived from rice husk [44, 48].

4.5 Scanning Electron Microscopy With Energy Dispersive Spectroscopy (SEM–EDX)

The present study employed scanning electron microscopy to examine the morphological characteristics of various materials, including phytolith (Fig. 5), ash particles at 650 °C

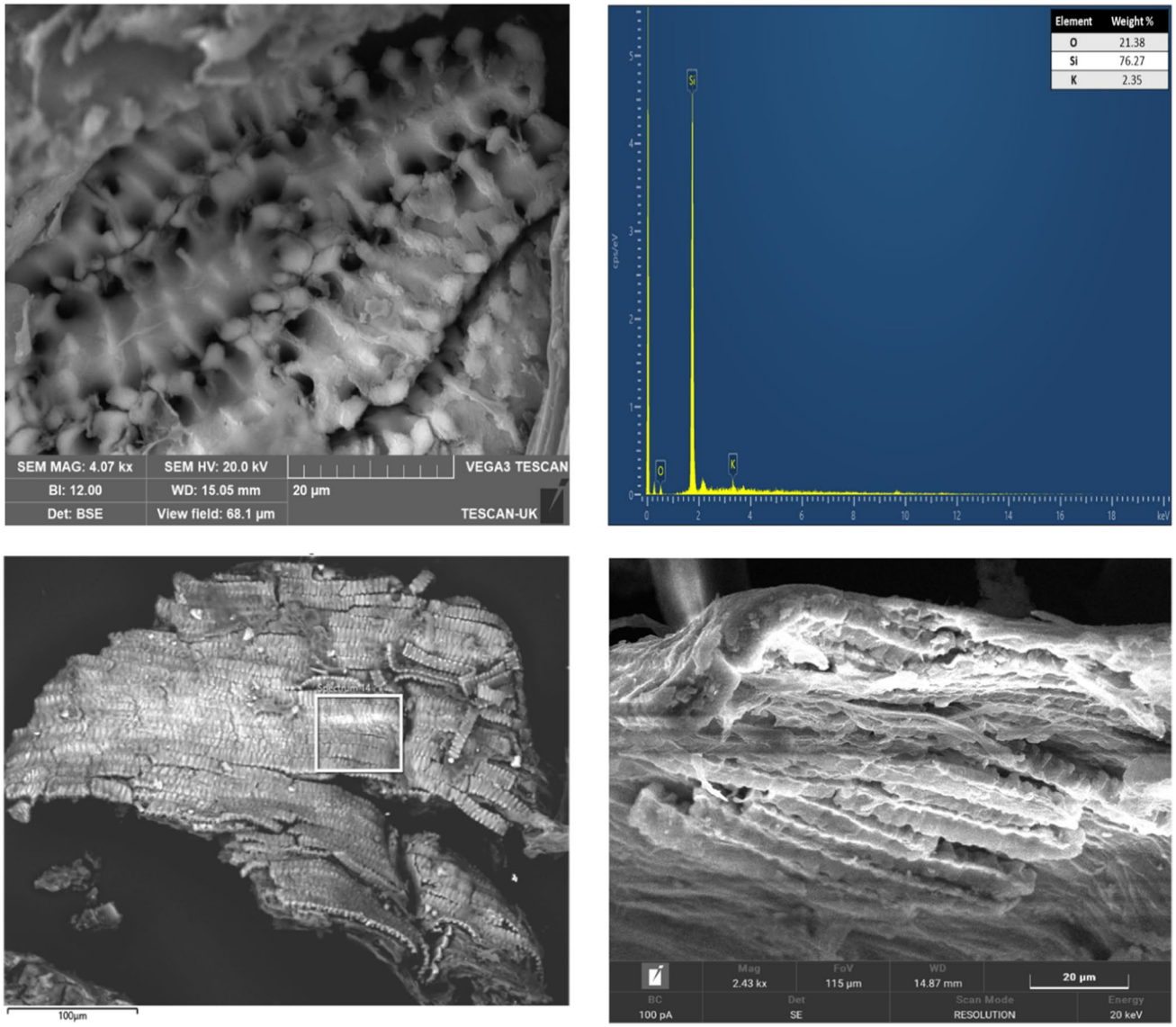

Fig. 5 SEM micrographs with EDX (20 and 100 µm) of phytolith in wheat biomass

(Fig. 6), ASi and CSi (Fig. 7). The phytolith structure present in wheat straw was observed in the form of articulated elongate undulate epidermal phytolith, which is consistent with phytoliths found in cereal taxa such as Triticeae and Aveneae [49]. These phytoliths are formed through cell wall silicification and are typically not thin, which aligns with observations in *Triticum aestivum*. Under light microscopy, dendritics are often echinate, thin, and heavily branched, with multiple extended lateral edges, whereas elongated and undulated phytoliths are formed under the presence of light microscopy, which represent wave patterns between boundaries of neighbouring cells [50, 51]. The silica skeleton was examined in various plants such as wheat, barley, rye grass, date palm, oat grass, and goat grass. Thin and thick waves were observed in long cells with round and irregular wave amplitude in wheat husks. The papillae found were large and overlapping in size, similar to the oblong-shaped papillae in *Triticum dicoccoides* of 8–10 µm diameter. The waves observed in the present microscopy are similar to the squarish thick cell wall with even wave amplitude [49, 50, 52–54]. These archaeological evidences require further research investigations to identify the ornamentation of papillae in wheat cultivars.

Moreover, energy dispersive spectroscopic (EDX) analysis was performed on several areas of the wheat straw biomass surface to determine its elemental composition. The obtained spectrum showed that silica (Si) constitutes 76.27% of the material, as revealed by the EDX analysis.

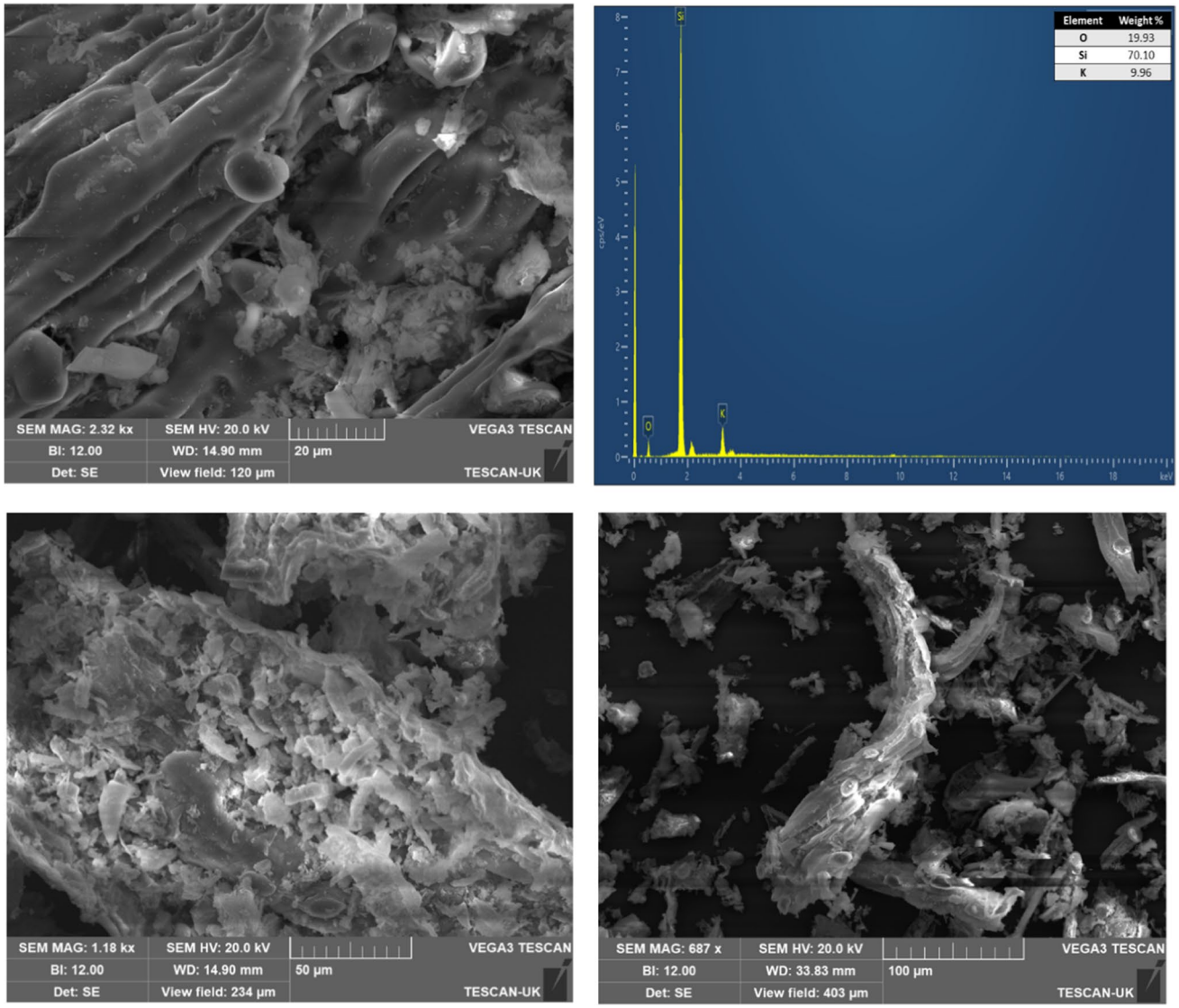

Fig. 6 SEM micrographs with EDX of wheat straw ash at 650 °C

Upon heating the wheat biomass at high temperatures, the resulting ash particles displayed irregular shapes and were agglomerated, indicating the complete removal of all organic content upon combustion at 650 °C. Figure 6 shows that the particle sizes ranged from small to large and featured several craters, revealing the surface roughness resulting from the removal of volatiles and organic constituents from the biomass.

The surface morphology observed in this study is similar to that observed in sugarcane waste ash [23]. Additionally, the EDX spectrum revealed a higher amount of silica (Si %) at 70.10%, with a minimal percentage of potassium (9.96%). The elemental Si present in the spectrum could be attributed to the indirect qualitative assessment of the ash as the source of Si. A study investigating the physical and chemical properties of biomass ash through microstructural analysis reported similar findings. The SEM micrographs presented in this study were consistent with those obtained when various biomass ashes, such as ground nut shells, rice husk, sugarcane bagasse, arecanut shells, and cashewnut shells, were heated at higher temperatures [55].

At magnifications ranging from 5 to 20 µm, the amorphous silica particles are seen to be highly agglomerated and are mostly spherical in shape, with a wide distribution. These micrographs closely resemble those of commercial silica, as illustrated in Fig. 7. The energy dispersive X-ray spectroscopy (EDX) analysis of the particles indicates a strong signal for both silicon (Si) and oxygen (O), with Si constituting 32.21% of the sample and O

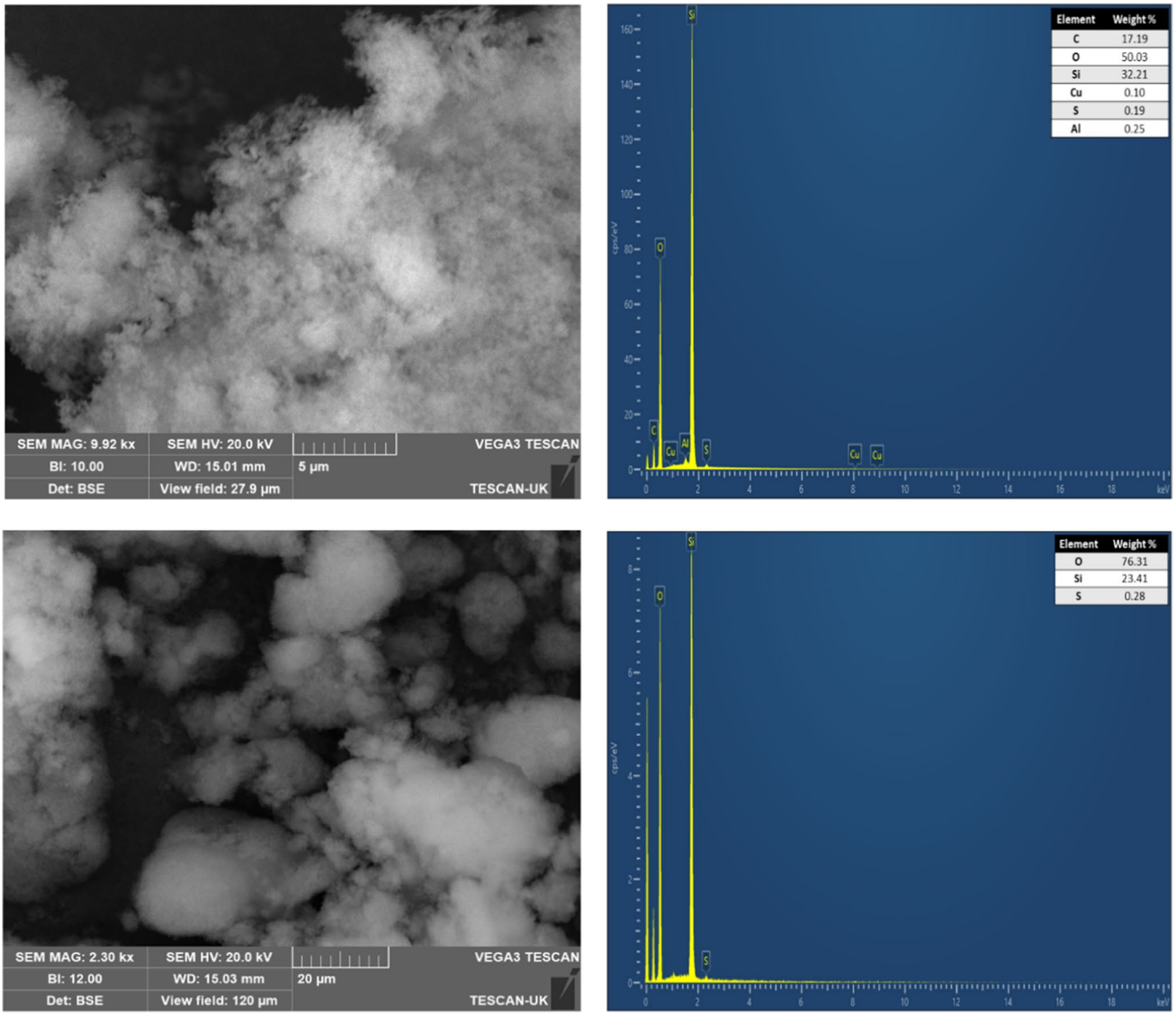

Fig. 7 SEM micrographs with EDX of ASi (top) and CSi (bottom)

constituting 50.03%. This confirms that the predominant component of the amorphous silica is SiO_2. It should be noted that the graphed elements reflect the substrates used during the analysis. The SEM images obtained are consistent with those of SiO_2 from palm kernel shells [40].

Based on the evidence presented, the presence of phytolith and SiO_2 in wheat straw suggests its potential for extraction and use in various applications. Additionally, exploring the potential of using agricultural residues as a sustainable source of silica to replace traditional sources, could contribute to a more environmentally friendly and circular economy. Furthermore, the presence of phytolith in wheat straw could also contribute to long-term terrestrial carbon sequestration [56].

4.6 Brunauer – Emmer –Teller (BET) Surface Area Analysis

In accordance with the IUPAC classification, the BET surface area measurements of amorphous silica revealed a type II isotherm curve with a hysteresis of H3 type, as demonstrated in Fig. 8. The graph depicted the hysteresis loop between the adsorption and desorption curves, indicating the mesoporous nature of the material with a size less than 50 nm. This H3 type is typically associated with slit-shaped pores formed by pellet aggregation, resulting in a broad pore distribution. However, the absence of a plateau in the relative pressure close to 1 indicates the lack of macroporosity.

The amorphous silica exhibited a wide pore distribution between 4 and 8, which indicated the existence of

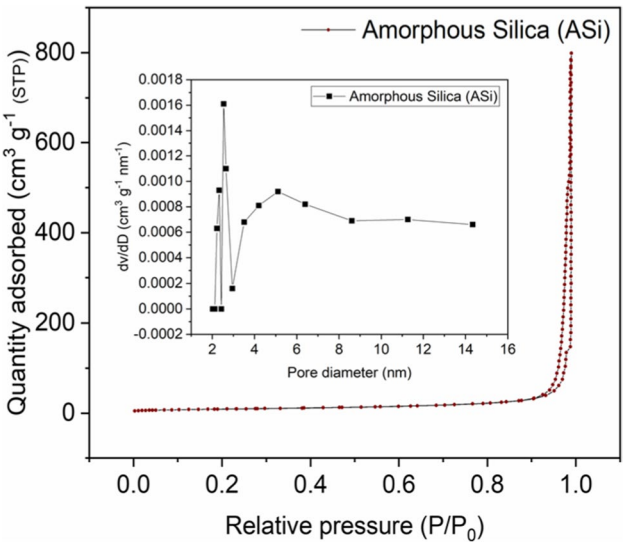

Fig. 8 N_2 Adsorption–desorption graph of ASi and Inset: Pore size distribution of ASi

mesopores, as illustrated in the inset of Fig. 8. Similarly, the porous silica derived from sugarcane waste ash showed mesoporous nature and exhibited the same hysteresis loop [23]. The results were also consistent with the nano silica produced from palm kernel [40].

The textural and surface area properties of ASi can be found in Table 5. Specifically, the data reported show that the ASi exhibit a substantial specific surface area covered with OH groups, which are especially reactive with H_2O, and other polar molecules. This fact implies the potential application of ASi in the adsorption of polar molecules. Additionally, the hydroxyl surface groups also permit the adsorption of nonpolar molecules such as CO_2 by forming weakly bonded adduct [57]. Based on the findings, ASi has the potential to be utilized as adsorbents in various applications. Hence, it has been demonstrated to be a potential adsorbent for capturing and separating CO_2 from flue gas emitted by power plants.

4.7 Thermogravimetric Analysis (TGA)

TGA was used to determine the thermal properties of wheat straw powder, ash, and amorphous silica. The weight loss curves were divided into four steps for better analysis of the mass change of the samples. The first stage of weight loss occurred between 25 °C and 150 °C, representing the removal of physically adsorbed moisture from all the samples (Fig. 9). In wheat straw, this was attributed to the hydrophilic nature of the straw and adsorbed solvents. This step indicated the dehydration and volatile release from all three materials.

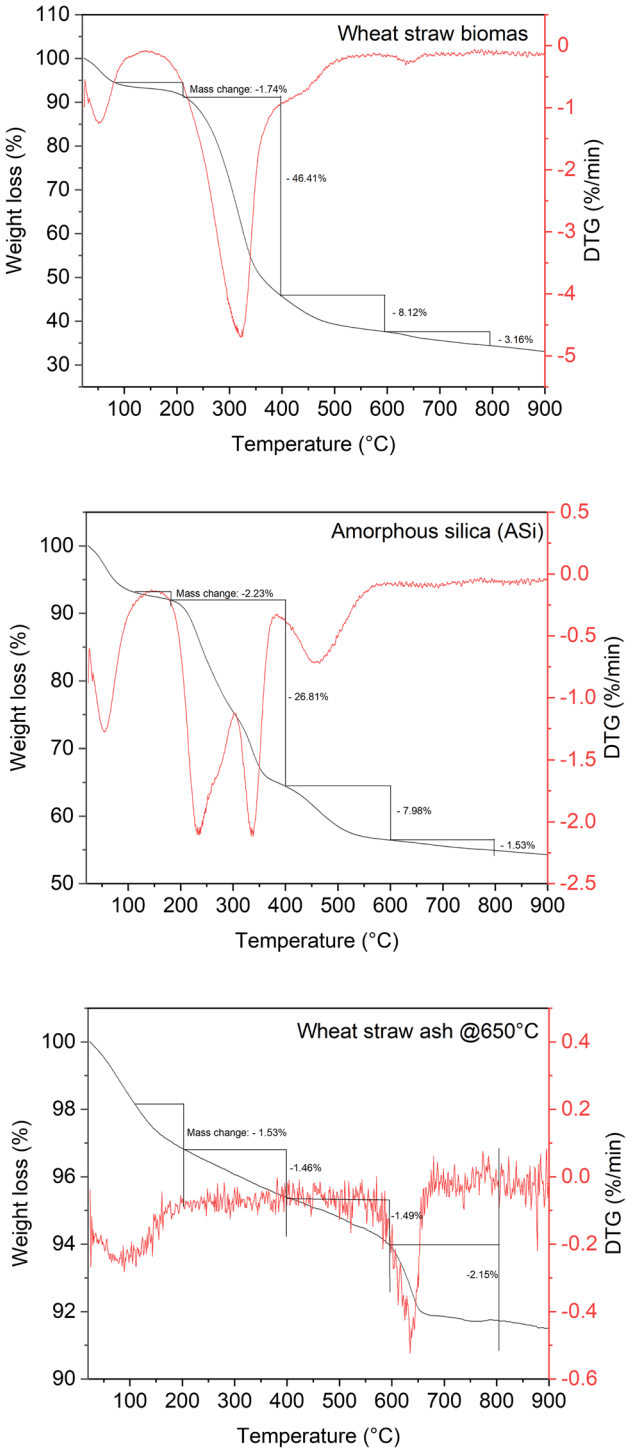

Fig. 9 TGA graph of wheat straw biomass, Amorphous silica (ASi) and wheat straw ash @650 °C

Table 5 Textural and surface area properties of ASi

Sample	S_{BET} /m^2 g^{-1}	d/nm	D_{BJH}/nm	V/cm^3 g^{-1}	V_T/cm^3 g^{-1}
ASi	32.045	154.216	187.994	0.013	1.235

*S_{BET}-BET surface area, d-average pore diameter, D_{BJH}-pore diameter, V-micropore volume, V_T-total pore volume

The second stage, between 150 °C and 400 °C, represented the decomposition of fiber. Hemicellulose degrades at 160 °C, and cellulose degrades between 220 °C and 380 °C. The highest weight loss was observed during this stage in wheat straw (-54.53%) and ASi (-34.79%). The negative sign in the graphs indicates the reduction in weight of each sample. The chemically bound water molecules during sol–gel process were removed from 150 °C to 600 °C in ASi [58]. Above 600 °C, no major weight loss was observed in any of the samples. During this temperature range, the degradation of remaining organic materials was noticed, but complex reactions were difficult to observe in the TGA/DTG curves [33, 59].

The increase in the amount of SiO_2 was reflected in the curves that corresponded to the thermal stability of the material. The higher mass loss was seen in stage two of wheat straw compared to the loss in ASi, while the least difference was observed in ash. Similar findings were observed for SiO_2 nanoparticles modified cellulose fibers [59], rice husk [33], palm kernel shells derived amorphous silica [40].

5 Conclusion

The utilization of agricultural residues, such as wheat straws, can create various opportunities for value addition. This study presents a novel approach for producing amorphous silica (ASi) from wheat straws using the modified sol–gel method and examines its physico-chemical properties. A modified extraction method has been identified, with optimized conditions of 3 M NaOH and 3 M H_2SO_4 at pH 9, resulting in the highest percentage of SiO_2 content in the ash produced at 650 °C ($30.20 \pm 0.09\%$) and biomass (34.41%). These findings indicate that wheat straw has potential as a source of silica extraction. The X-Ray Diffraction (XRD) spectrum of ash at 650 °C confirmed the amorphous nature of the particles, and the qualitative EDX assessment indicated that the percentage SiO_2 in wheat straw was approximately 77%. The Fourier transform infrared spectroscopic (FTIR) graphs revealed the presence of silanol groups (Si–O-Si) at a wavenumber of 400–800 cm^{-1}. The BET surface area and pore volume of ASi were estimated to be 32.045 $m^2\ g^{-1}$ and 1.235 $cm^3\ g^{-1}$, respectively, with a mesoporous pore distribution of 154.216 nm. These results suggest that ASi has potential for various environmental applications. Moreover, surface modifications could be explored for desired applications such as adsorbent, catalyst and others.

In terms of economics, compared to physical and other chemical methods, the sol–gel method used to extract silica from wheat straw can be considered a better alternative. While it may be more expensive than some of the other methods, it has several advantages:

1. It is a more controlled and efficient method, resulting in a higher yield of pure silica.
2. The sol–gel method can be used to produce silica nanoparticles with a uniform size, which can be useful for certain applications.
3. It does not require the use of hazardous chemicals, making it safer for workers and the environment.

Overall, while the sol–gel method may have some drawbacks, it is still considered a better alternative to many of the other methods of silica extraction from biomass. Moreover, research is essential to improve and optimize the sol–gel method to make it more cost-effective and environmentally friendly.

Acknowledgements We are very grateful to Cranfield University, United Kingdom for granting visiting fellowship and provision of the laboratory used for this research. Our sincere appreciation for the support and facilitation by Tamil Nadu Agricultural University, Coimbatore, India. The fantastic support provided by the technicians (Cristinel Putinica, Nuannat Simmons, Richard Andrews, Paul Barton, Christine Kimpton, Diane Johnson) at Cranfield University is also very appreciated by the authors.

Author Contribution Sangeetha Ramasamy: Conceptualization, Data curation, Formal analysis, Investigation, Methodology, Validation, Visualization, Writing—original draft. Ruben Sakrabani: Conceptualisation, Investigation, Methodology, Writing – Review & Editing, Funding acquisition, Project administration, Resources, Supervision. Sadish Oumabady: Investigation, Writing—original draft. Davamani Veeraswamy, Parameswari Ettiyagounder, Lakshmanan Arunachalam, Sivakumar Senjeriputhur Devaraj, Kadirvelu Krishna: Writing – review & editing.

Funding The authors wish to thank the support of the Commonwealth Scholarship Commission, United Kingdom [No.INCN-2021–118] and the Department of Science and Technology (DST-SERB), New Delhi, India [No.DST/INSPIRE/03/2021/001372] for the research funding.

Data Availability All data generated or analysed during this study are included in this published article.

Declarations

Ethical Approval Authors have been granted ethical approval before carrying out this project.

Consent to Participate All authors have given consent to participate.

Consent for Publication All authors read and approved the final manuscript.

Competing Interests The authors declare no competing interests.

References

1. Sun M, Xu X, Wang C et al (2020) Environmental burdens of the comprehensive utilization of straw: Wheat straw utilization from a life-cycle perspective. J Clean Prod 259:120702. https://doi.org/10.1016/j.jclepro.2020.120702
2. Bartocci P, Zampilli M, Liberti F et al (2020) LCA analysis of food waste co-digestion. Sci Total Environ 709:136187. https://doi.org/10.1016/j.scitotenv.2019.136187
3. Li S, Chen G (2020) Agricultural waste-derived superabsorbent hydrogels: Preparation, performance, and socioeconomic impacts. J Clean Prod 251:119669
4. Ingrao C, Matarazzo A, Gorjian S et al (2021) Wheat-straw derived bioethanol production: A review of Life Cycle Assessments. Sci Total Environ 781:146751
5. Shafer M (2020) Global crop waste burning – micro-biochar; how a small community development organization learned experientially to address a huge problem one tiny field at a time. Sustain Earth 3:1–14. https://doi.org/10.1186/s42055-020-00037-y
6. Usmani M, Kondal A, Wang J, Jutla A (2020) Environmental Association of Burning Agricultural Biomass in the Indus River Basin. GeoHealth 4:. https://doi.org/10.1029/2020GH000281
7. Ingrao C, Failla S, Arcidiacono C (2020) A comprehensive review of environmental and operational issues of constructed wetland systems. Curr Opin Environ Sci Heal 13:35–45
8. Salazar Hoyos LA, Faroldi BM, Cornaglia LM (2020) A coke-resistant catalyst for the dry reforming of methane based on Ni nanoparticles confined within rice husk-derived mesoporous materials. Catal Commun 135:105898. https://doi.org/10.1016/j.catcom.2019.105898
9. Davamani V, Sangeetha Piriya R, Rakesh SS et al (2022) Phytolith-Occluded Carbon Sequestration Potential of Oil Palm Plantation in Tamil Nadu. ACS Omega 7:2809–2820. https://doi.org/10.1021/acsomega.1c05592
10. Xue B, Jin L, Chen Z et al (2019) The template effect of silica in rice husk for efficient synthesis of the activated carbon based electrode material. J Alloys Compd 789:777–784. https://doi.org/10.1016/j.jallcom.2019.03.012
11. Roselló J, Soriano L, Santamarina MP et al (2015) Microscopy Characterization of Silica-Rich Agrowastes to be used in Cement Binders: Bamboo and Sugarcane Leaves. Microsc Microanal 21:1314–1326. https://doi.org/10.1017/S1431927615015019
12. Huang SS, Tung MT, Huynh CD et al (2019) Engineering Rice Husk into a High-Performance Electrode Material through an Ecofriendly Process and Assessing Its Application for Lithium-Ion Sulfur Batteries. ACS Sustain Chem Eng 7:7851–7861. https://doi.org/10.1021/acssuschemeng.9b00092
13. Damanhuri AAM, Lubis AMHS, Hariri A, et al (2020) Mechanical properties of Rice husk ash (RHA) brick as partial replacement of clay. In: Journal of Physics: Conference Series. IOP Publishing, Bristol, p 042034. https://iopscience.iop.org/article/10.1088/1742-6596/1529/4/042034
14. Shim J, Velmurugan P, Oh BT (2015) Extraction and physical characterization of amorphous silica made from corn cob ash at variable pH conditions via sol gel processing. J Ind Eng Chem 30:249–253. https://doi.org/10.1016/j.jiec.2015.05.029
15. Okoronkwo EA, Imoisili PE, Olisunle SOO (2013) Extraction and characterization of Amorphous Silica from Corn Cob Ash by Sol-Gel Method | Okoronkwo | Chemistry and Materials Research. Chem Mater Res 3:68–72
16. Falk G, Shinhe GP, Teixeira LB et al (2019) Synthesis of silica nanoparticles from sugarcane bagasse ash and nano-silicon via magnesiothermic reactions. Ceram Int 45:21618–21624. https://doi.org/10.1016/j.ceramint.2019.07.157
17. Osman NS, Sapawe N (2020) Preparation of amorphous oil palm frond ash (OPFA) via acid leaching treatment as precursor for silica synthesis. In: Materials Today: Proceedings. Elsevier, Amsterdam, pp 253–256. https://doi.org/10.1016/j.matpr.2020.05.333
18. Grimm AM, Dorsch LY, Kloess GH et al (2021) Transition metal promoted combustion of rice husk and rice straw towards an energy optimized synthesis of biogenic silica. Biomass Bioenergy 155:106282. https://doi.org/10.1016/j.biombioe.2021.106282
19. He Z, Li Y, Liu C et al (2021) Controllable conversion of biomass to lignin-silica hybrid nanoparticles: High-performance renewable dual-phase fillers. Waste Manag 135:381–388. https://doi.org/10.1016/j.wasman.2021.09.025
20. Bakar RA, Yahya R, Gan SN (2016) Production of High Purity Amorphous Silica from Rice Husk. Procedia Chem 19:189–195. https://doi.org/10.1016/j.proche.2016.03.092
21. Ng EP, Chow JH, Mukti RR et al (2017) Hydrothermal synthesis of zeolite a from bamboo leaf biomass and its catalytic activity in cyanoethylation of methanol under autogenic pressure and air conditions. Mater Chem Phys 201:78–85. https://doi.org/10.1016/j.matchemphys.2017.08.044
22. Athinarayanan J, Jaafari SAAH, Periasamy VS et al (2020) Fabrication of Biogenic Silica Nanostructures from Sorghum bicolor Leaves for Food Industry Applications. SILICON 12:2829–2836. https://doi.org/10.1007/s12633-020-00379-4
23. Rovani S, Santos JJ, Corio P, Fungaro DA (2018) Highly Pure Silica Nanoparticles with High Adsorption Capacity Obtained from Sugarcane Waste Ash. ACS Omega 3:2618–2627. https://doi.org/10.1021/acsomega.8b00092
24. Imoisili PE, Ukoba KO, Jen TC (2020) Green technology extraction and characterisation of silica nanoparticles from palm kernel shell ash via sol-gel. J Mater Res Technol 9:307–313. https://doi.org/10.1016/j.jmrt.2019.10.059
25. Chindaprasirt P, Rattanasak U (2020) Eco-production of silica from sugarcane bagasse ash for use as a photochromic pigment filler. Sci Rep 10:1–8. https://doi.org/10.1038/s41598-020-66885-y
26. Domingues RR, Trugilho PF, Silva CA et al (2017) Properties of biochar derived from wood and high-nutrient biomasses with the aim of agronomic and environmental benefits. PLoS One 12:e0176884. https://doi.org/10.1371/journal.pone.0176884
27. Piriya RS, Jayabalakrishnan RM, Maheswari M et al (2021) Coconut shell derived ZnCl2activated carbon for malachite green dye removal. Water Sci Technol 83:1167–1182. https://doi.org/10.2166/wst.2021.050
28. Wadi B, Golmakani A, Manovic V, Nabavi SA (2021) Effect of combined primary and secondary amine loadings on the adsorption mechanism of CO2 and CH4 in biogas. Chem Eng J 420:130294. https://doi.org/10.1016/j.cej.2021.130294
29. Sharma RK, Sharma S, Dutta S et al (2015) Silica-nanosphere-based organic-inorganic hybrid nanomaterials: Synthesis, functionalization and applications in catalysis. Green Chem 17:3207–3230. https://doi.org/10.1039/C5GC00381D
30. Nizamuddin S, Qureshi SS, Baloch HA et al (2019) Microwave hydrothermal carbonization of rice straw: Optimization of process parameters and upgrading of chemical, fuel, structural and thermal properties. Materials (Basel) 12:403. https://doi.org/10.3390/ma12030403

31. Kow KW, Yusoff R, Aziz ARA, Abdullah EC (2014) Characterisation of bio-silica synthesised from cogon grass (Imperata cylindrica). Powder Technol 254:206–213. https://doi.org/10.1016/j.powtec.2014.01.018
32 Sarwar A, Ali M, Khoja AH et al (2021) Synthesis and characterization of biomass-derived surface-modified activated carbon for enhanced CO2adsorption. J CO2 Util 46:101476. https://doi.org/10.1016/j.jcou.2021.101476
33. Santana Costa JA, Paranhos CM (2018) Systematic evaluation of amorphous silica production from rice husk ashes. J Clean Prod 192:688–697. https://doi.org/10.1016/j.jclepro.2018.05.028
34. Ikubanni PP, Oki M, Adeleke AA et al (2020) Influence of temperature on the chemical compositions and microstructural changes of ash formed from palm kernel shell. Results Eng 8:100173. https://doi.org/10.1016/j.rineng.2020.100173
35. Varkouhi S, Wells J (2020) The relation between temperature and silica benthic exchange rates and implications for near-seabed formation of diagenetic opal. Results Geophys Sci 1–4:100002. https://doi.org/10.1016/j.ringps.2020.100002
36. Boström D, Skoglund N, Grimm A et al (2012) Ash transformation chemistry during combustion of biomass. Energy Fuels 26:85–93. https://doi.org/10.1021/ef201205b
37. Lu P, Lo HY (2012) Highly pure amorphous silica nano-disks from rice straw. Powder Technol 225:149–155. https://doi.org/10.1016/j.powtec.2012.04.002
38. Nandiyanto ABD, Rahman T, Fadhlulloh MA, et al (2016) Synthesis of silica particles from rice straw waste using a simple extraction method. In: IOP Conference Series: Mater Sci Eng IOP Publishing, p 012040
39. Liu ZS, Li WK, Huang CY (2014) Synthesis of mesoporous silica materials from municipal solid waste incinerator bottom ash. Waste Manag 34:893–900. https://doi.org/10.1016/j.wasman.2014.02.016
40. Imoisili PE, Ukoba KO, Jen TC (2020) Synthesis and characterization of amorphous mesoporous silica from palm kernel shell ash. Bol la Soc Esp Ceram y Vidr 59:159–164. https://doi.org/10.1016/j.bsecv.2019.09.006
41. Ali A, Chiang YW, Santos RM (2022) X-Ray Diffraction Techniques for Mineral Characterization: A Review for Engineers of the Fundamentals, Applications, and Research Directions. Minerals 12:205. https://doi.org/10.3390/min12020205
42. Madejová J (2003) FTIR techniques in clay mineral studies. Vib Spectrosc 31:1–10
43. Carmona VB, Oliveira RM, Silva WTL et al (2013) Nanosilica from rice husk: Extraction and characterization. Ind Crops Prod 43:291–296. https://doi.org/10.1016/j.indcrop.2012.06.050
44. Adediran AA, Alaneme KK, Oladele IO, Akinlabi ET (2018) Processing and structural characterization of Si-based carbothermal derivatives of rice husk. Cogent Eng 5:1–12. https://doi.org/10.1080/23311916.2018.1494499
45. Björklund S, Kocherbitov V (2017) Alcohols react with MCM-41 at room temperature and chemically modify mesoporous silica. Sci Rep 7:1–11. https://doi.org/10.1038/s41598-017-10090-x
46. Iler RK (1979) The chemistry of silica: solubility, polymerization, colloid and surface properties, and biochemistry. Lavoisierfr 892 pp. https://doi.org/10.1002/ange.19800920433
47. Kocherbitov V, Alfredsson V (2007) Hydration of MCM-41 studied by sorption calorimetry. J Phys Chem C 111:12906–12913. https://doi.org/10.1021/jp072474r
48. Ali M, Tindyala MA (2015) Thermoanalytical studies on acid-treated rice husk and production of some silicon based ceramics from carbonised rice husk. J Asian Ceram Soc 3:311–316. https://doi.org/10.1016/j.jascer.2015.06.003
49. Ball TB, Gardner JS, Anderson N (1999) Identifying inflorescence phytoliths from selected species of wheat (Triticum monococcum, T. Dicoccon, T. Dicoccoides, and T. Aestivum) and barley (Hordeum vulgare and H. Spontaneum) (Gramineae). Am J Bot 86:1615–1623. https://doi.org/10.2307/2656798
50. Rosen AM (1992) Preliminary Identification of Silica Skeletons from Near Eastern Archaeological Sites: An Anatomical Approach. Phytolith Systematics. Springer, US, pp 129–147
51. Ball T, Vrydaghs L, Mercer T et al (2017) A morphometric study of variance in articulated dendritic phytolith wave lobes within selected species of Triticeae and Aveneae. Veg Hist Archaeobot 26:85–97. https://doi.org/10.1007/s00334-015-0551-x
52. Shillito LM (2011) Taphonomic observations of archaeological wheat phytoliths from neolithic çatalhöyük, Turkey, and the use of conjoined phytolith size as an indicator of water availability. Archaeometry 53:631–641. https://doi.org/10.1111/j.1475-4754.2010.00582.x
53. Rashid I, Mir SH, Zurro D et al (2019) Phytoliths as proxies of the past. Earth-Science Rev 194:234–250
54. Ball T, Gardner JS, Brotherson JD (1996) Identifying phytoliths produced by the inflorescence bracts of three species of wheat (Triticum monococcum L., T. dicoccon Schrank., and T. aestivum L.) using computer-assisted image and statistical analyses. J Archaeol Sci 23:619–632. https://doi.org/10.1006/jasc.1996.0058
55. Umamaheswaran K, Batra VS (2008) Physico-chemical characterisation of Indian biomass ashes. Fuel 87:628–638. https://doi.org/10.1016/j.fuel.2007.05.045
56. Davamani V, Sangeetha Piriya R, Rakesh SS, et al (2022) Phytolith-Occluded Carbon Sequestration Potential of Oil Palm Plantation in Tamil Nadu. ACS Omega acsomega.1c05592. https://doi.org/10.1021/acsomega.1c05592
57. Roque-Malherbe R, Polanco-Estrella R, Marquez-Linares F (2010) Study of the interaction between silica surfaces and the carbon dioxide molecule. J Phys Chem C 114:17773–17787. https://doi.org/10.1021/jp107754g
58. Mueller R, Kammler HK, Wegner K, Pratsinis SE (2003) OH surface density of SiO2 and TiO2 by thermogravimetric analysis. Langmuir 19:160–165. https://doi.org/10.1021/la025785w
59. Raabe J, De Souza FA, Bufalino L et al (2014) Evaluation of reaction factors for deposition of silica (SiO2) nanoparticles on cellulose fibers. Carbohydr Polym 114:424–431. https://doi.org/10.1016/j.carbpol.2014.08.042